High resolution core level photoemission of clean and adsorbate covered metal surfaces

2001 J. Phys.: Condens. Matter 13 11267

(http://iopscience.iop.org/0953-8984/13/49/311)

INSTITUTE OF PHYSICS PUBLISHING JOURNAL OF PHYSICS: CONDENSED MATTER

J. Phys.: Condens. Matter **13** (2001) 11267–11291 PII: S0953-8984(01)28903-6

High resolution core level photoemission of clean and adsorbate covered metal surfaces

Jesper N Andersen[1] **and Carl-Olof Almbladh**[2]

[1] Department of Synchrotron Radiation Research, Institute of Physics, Lund University, Box 118, S-221 00 Lund, Sweden
[2] Department of Solid State Theory, Institute of Physics, Lund University, Box 118, S-221 00 Lund, Sweden

Received 18 September 2001, in final form 13 November 2001
Published 10 December 2001
Online at stacks.iop.org/JPhysCM/13/11267

Abstract

A brief review is given of some fundamental aspects of high-resolution core-level photoemission and of its application to studies of pure and adsorbate covered metal surfaces. We first give a short description of the basic theory and then turn to a number of examples. The first group of examples is aimed at demonstrating the use of core-level binding energy shifts for deriving the surface and interface geometrical structure whereas the second group deals with the core-level lineshape and, in particular, the influence of vibrational and other excitations.

1. Introduction

Core-level photoemission has proved to be a very popular and valuable method for studying many of the properties of the surface region of solids, see e.g. [1] and references therein. Fundamental reasons for this are the inherent element specificity due to the element specific core-level binding energies, the quantitative dependence of the core-level photoemission signal on the amount of elements present, and the surface sensitivity caused by the short mean free path of low energy electrons in solids. Thus at the most basic level, core-level photoemission offers a determination of the elemental composition in the surface region. Measurements at this level do not require particular high-energy resolution as the core-level binding energies of different elements normally differ substantially. If, however, the measurements are performed at sufficiently high energy resolution it is often possible to detect that the core-level binding energies of a particular element show small shifts if that element is placed in different surroundings. Due to these small shifts of the core-level binding energies induced by changes in the surroundings of the emitting atom, core-level photoemission is said to be also chemically specific. The discovery of these so-called 'chemical shifts' formed the basis for the well known electron spectroscopy for chemical analysis (ESCA) [2] technique. The chemical shifts of the core-level binding energies have proved to be very useful in surface studies as

they allow for a separation of the various inequivalent kinds of atoms of the elements found in the near surface region. Atoms in the first atomic layer of a surface experience a different environment than atoms in deeper layers and the resulting core-level binding energy shift allows for a separation of the surface signal whereby the behaviour of the outermost atomic layer may be monitored separate from that of the bulk. The core-level binding energies of adsorbates, atomic and molecular, likewise depend on the surroundings of the adsorbate and thus core-level photoemission may provide information on the number of inequivalent atoms/molecules in an adsorption system. These shifts of the adsorbate core levels may, at various levels of sophistication, be used to provide useful fingerprints of e.g. adsorption sites, dissociation of adsorbed molecules, and intermixing with the substrate. An analysis of the adsorbate and the substrate core-level binding energy shifts may in favourable cases be used to obtain a determination of the adsorption site. Even in cases where this may not be possible, the combination of adsorbate and substrate core-level binding energy shifts often puts severe limits on the possible structural models thereby limiting greatly the number of such models which have to be considered by other methods. Although a chemical shift should always result when a change occurs in the surroundings of an atom, these shifts may in many cases be very small. Detection of smaller and smaller chemical shifts has been one of the major driving forces for increasing the experimental energy resolution in core-level photoemission. In addition to allowing for the measurement of small binding energy shifts, improvements of the energy resolution also allow for accurate studies of the detailed lineshape of the core-level photoemission peaks. This lineshape carries information on the dynamical response of the systems electronic and nuclear degrees of freedom to the sudden creation of a core hole and its subsequent decay. A detailed understanding of the effects, which influence the core-level lineshape, has proved to be vital for a correct decomposition of high-resolution core photoemission spectra.

In this short review we first give a brief description of some fundamental ingredients in a theoretical description of core-level photoemission from metallic solids. We then proceed with several examples of the use of core-level binding energy shifts in studies of pure metal and adsorbate covered surfaces. After this we turn to experimental results concerning the core-level lineshapes and the information contained in these. In this part we concentrate on structure caused by excitation of the nuclear degrees of freedom, i.e. vibrations, in the core-level photoemission process. We have not intended to give an exhaustive review of the litterature and the chosen examples (and the reference list) are highly biased towards results that have originated in our research groups.

2. Core-level photoemission

In a core-level photoemission experiment the binding energy, $E_B = -\varepsilon_c$, of a particular core-level 'c' is determined by letting photons of well defined energy impinge upon a sample followed by a determination of the kinetic energy of the emitted core electrons by an energy analyser. The binding energy is then defined as $\hbar\omega - E_{kin}$ where, in the case of metallic samples, the zero of the energy scale refers to the Fermi level. Equivalently, the core-electron energy may be defined as the difference in total energy of the sample after and before the emission, i.e. the total energy difference between the final (f) and the initial (i) state, $\varepsilon_c = E_f - E_i$. As will be touched upon later, a number of final states may be reached and thus the core-level peak has a certain width. The core-level excitations have a special structure with a usually rather well defined high-energy threshold or 'lowest binding energy' corresponding to a fully relaxed core-hole state. We will take this threshold as the definition of the core-electron energy ε_c.

The notion of 'lowest binding energy' for a core level, or a fully relaxed core-hole state,

implicitly refers to an approximate zero-order scheme where all lifetime effects are neglected. The electron–electron interaction involves couplings between a particular core-level 'c' and the valence electrons which conserve the core-level occupancy and terms which cause transitions between different shells. The latter terms give rise to Auger and Coster–Kronig transitions and a finite core-hole lifetime. Also the coupling to photons gives intershell transitions resulting in radiative core-hole decay. To leading order these Auger and radiative terms just result in an additional Lorentzian broadening of the infinite lifetime spectrum (see e.g. [3, 4]). For core holes with binding energies in the range up to a few keV the lifetime width is typically of the order tenths of an eV and thus small on an electronic energy scale. Turning to the core-level conserving part of the interaction, it gives relaxation shifts (typically of the order 5–10 eV) and causes shake-ups such as plasmon satellites and asymmetries arising from electron–hole pairs. This part of the interaction is of the form

$$\sum_{k,k'} \left[\langle kc|v|k'c\rangle - \langle kc|v|ck'\rangle \right] c_k^+ b^+ b c_{k'}. \tag{1}$$

Here v is the bare Coulomb interaction, the electron operator b refers to the core-level under consideration, and c_k, $c_{k'}$ refer to valence states (or to other core shells). By writing $b^+b = 1 - bb^+$ we obtain one part which acts on the ground state and an additional part Vbb^+ which acts on the valence electrons when the core level is unoccupied. The electronic part of V is of the form

$$V_{el} = \sum \langle k|w|k'\rangle c_k^+ c_{k'}$$

with

$$\langle k|\, w|k'\rangle = -\left[\langle kc|\, v|k'v\rangle - \langle kc|\, v|ck'\rangle \right].$$

The first direct term in w dominates over the second exchange term. Keeping only the direct term, w becomes a local attractive potential,

$$w(\boldsymbol{r}) = -\int \mathrm{d}^3 r' v(\boldsymbol{r} - \boldsymbol{r}') \left|\phi_c(\boldsymbol{r}')\right|^2.$$

We notice that it is a bare Coulomb interaction which enters in w. The screening is provided by the valence electrons.

The definition of the binding energy as the total energy difference between the (ground states of the) final and the initial state forms the basis for calculations of binding energies and in particular binding energy shifts in metallic systems. In principle what is needed for describing the chemically shifted components of a particular element in a sample are calculations of the initial system total energy and of the various final states corresponding to the core hole being localized on the various chemically inequivalent atoms. Such total energy calculations can be made in several ways. An extensive amount of work is based on the so-called thermo-chemical approach as put forward for metallic systems by Johansson and Mårtensson [5]. A basic ingredient in this approach is the realization that, from the viewpoint of the valence electrons, the creation of a core hole is similar to adding an extra proton to the nucleus. Applying this 'equivalent core' or '$Z + 1$' approximation in connection with various Born–Haber cycles, the core-level binding energy shifts can be related to various thermodynamical properties of the $Z/Z + 1$ metal combination, see e.g. [1, 5–7]. These properties are in some cases measurable by other techniques or they may be calculated e.g. by the use of Miedema's semi-empirical methods [8] allowing for estimates of the expected shifts. Alternatively, experimental determinations of the core-level binding energy shifts may be seen as a means to measure thermodynamical properties, like e.g. surface and interface segregation energies, which are hard to access by other techniques. We will not go into details with these uses of core-level

photoemission in the present brief review but refer the reader to the literature e.g. the reviews by Egelhoff [1] and Mårtensson and Nilsson [7]. Here we simply note that these thermo-chemical models in our opinion provide very valuable means for 'back of the envelope' estimates of the magnitude of the core-level binding energy shifts to expect and for measurements of certain thermodynamic parameters.

The total energies of the sample before and after the core ionization may alternatively be calculated with a high level of accuracy by *ab initio* methods based on density functional theory (DFT) [9]. At first sight it may seem surprising that ground-state DFT can be used at all for obtaining the energies of the highly excited core-hole states. However, the fully relaxed hole state looks like a ground state as far as the valence electrons are concerned. Some formal justification can be obtained by considering DFT in subspaces, where in this case each ion core configuration would define a subspace. In principle, the density functional would depend on the occupancy n_c of particular core level under consideration, but this dependence is highly transferable and may be estimated from some reference system such a free atom or ion. Often the interest is focused on calculation of the binding energy shifts, as opposed to absolute values of the binding energies, of inequivalent atoms in a solid. In such calculations of the chemical shifts, where the core hole is sequentially placed on the different chemically inequivalent atoms and the total energy differences calculated, the dependence on n_c and possible systematic errors in the total energy differences between the initial and the final state are largely expected to cancel thereby improving the accuracy. This expectation is borne out by experience. In principle the calculation for the final state system involves a calculation of a single isolated 'impurity'. This breaks translational symmetry and thereby prohibits the use of conventional codes for total energy calculations of solids. Although calculations which treat the core-ionized atom as an isolated impurity have been performed [10], a more common approach to surface related calculations reintroduces translational symmetry by describing the metal as a thin slab and arranging the ionized final state impurity atoms in a supercell. In these approaches, thin repeated slabs of the structure under study are separated by vacuum layers thick enough to avoid interaction between the slabs whereas in the plane of the slabs a large 2D supercell is chosen for the ionized atoms. The convergence of the calculated core-level binding energy shifts with respect to these parameters (and of course also other parameters of a more technical nature) can be checked by simply varying them and explicitly calculating the core-level shifts. A very welcome (and expected) outcome of such convergence checks is that for metallic systems, the size of the 2D unit cells required is quite small due to the short screening length of the core hole in a metallic system. Part of the reason for the small size of the 2D unit cells required presumably also relies on the fact that if interactions exist between core holes they may be expected to be rather similar for the various inequivalent atoms of the solid and therefore the effect of such interactions will cancel when the shifts are calculated.

These *ab initio* calculations are very flexible when it comes to the chemical and structural properties of the solids as almost any composition and structure can be specified in a calculation. For example, for investigations of alloy core-level shifts, a large range of alloy compositions can be calculated and compared to experiment with the aim of identifying which alloys are present at the surface. The calculated core-level binding energy shifts are not only sensitive to gross features like structure and composition of the solid but also to finer geometrical parameters like interatomic distances [11]. This means that realistic values of the interatomic distances have to be used in the calculations if a high degree of accuracy is required for the core-level shifts. Thus a common procedure is to first optimize the geometry of the unionized initial state and subsequently use this geometry as input for the final state calculation. We usually use a generalized gradient approximation (GGA) for the exchange-correlation potential as this normally results in values for the geometrical parameters closer to experiment than

those obtained by the use of the local density approximation (LDA) (For reviews of current approximations in DFT see [12].) However, at fixed geometry the core-level energies are usually quite insensitive to the approximation used for exchange and correlation. Whereas this need for optimization of the geometry often increases the computational time considerably, the influence of the detailed geometry on the core-level binding energy shifts on the other hand means that these geometrical details in favourable cases may be derived from the core-level shifts.

The core-level lineshape carries valuable information about the excited states. In photoemission from solids the photoelectron has to travel through the system and pass the surface before it finally hits the detector. During this transport, the photoelectron may exchange energy with the system and this energy exchange will influence the observed lineshapes. When the spectra are excited well above threshold, however, the sudden approximation [13–15] is believed to apply. In this approximation we regard the photoemission as a sudden removal of a core electron, and the effects of the transport out of the system ('extrinsic effects') are added separately, in the spirit of Spicer's three-step model [16]. The central quantity is then the core-electron spectral function $A_c(\varepsilon)$, which describes the spectral distribution of final states after a sudden removal of a core electron. Neglecting lifetime effects we can classify the states after the core-level occupancy into no-hole states $|s\rangle$ and core-hole states $|s*\rangle$ and we can write the spectrum as

$$A_c(\varepsilon) = \sum_{fi} g_i |\langle f, *|i\rangle|^2 \delta(\varepsilon + E_f^* - E_i) \tag{2}$$

where we have allowed for finite temperatures via statistical weights g_i. The valence electron part of the spectrum will then involve overlaps between the ground state and excited states with a core-hole impurity. In free-electron-like systems, the excited states reached involve particle-hole excitation, which give rise to the well known Mahan–Nozières–DeDominicis asymmetry [17] and collective excitations giving plasmon satellites.

To include effects of lattice vibrations we assume the Born–Oppenheimer approximation [18] and let each electronic state depend on the position $\boldsymbol{R}$ of all the nuclei. We further assume that all electronic states near the core threshold have the same $\boldsymbol{R}$ dependence as the fully relaxed state $|0*\rangle$ and neglect a possible $\boldsymbol{R}$ dependence of transition matrix elements (the 'Condon' approximation [18]). Within these approximations the effect of lattice vibrations enters as a broadening function $D_{ph}(\hbar\omega)$, which gives the complete spectrum when convoluted with the spectrum A_{el}arising from only the electrons (see e.g. [3, 18]). The phonon broadening is again of the same form as in (2), but with vibronic states Φ_n^*, Φ_n with and without a core-hole impurity,

$$D_{ph}(\hbar\omega) = \sum_{fi} g_i |\langle \Phi_n^* | \Phi_i \rangle|^2 \delta(\hbar\omega + \hbar\Omega_f^* - \hbar\Omega_i). \tag{3}$$

In the harmonic approximation the initial and final vibronic states follows from harmonic oscillator Hamiltonians and the phonon broadening function may be calculated exactly. The main problem is to determine the dynamical matrices in the initial and final electronic states. Here, DFT has proven to yield rather accurate results [19].

Usually the phonon coupling (V_{ph}) to the core hole is dominated by the leading terms which are linear in lattice displacements, $V_{ph} = \sum B_\nu a_\nu + B_\nu^+ a_\nu^+$. The core hole will then not mix different modes ν or change the vibrational frequenciesω_ν. The formal solution has been well known for many years and is most conveniently written in time space,

$$D_{ph}(t) = \exp\left\{ \int_0^\infty g(\omega) \left[-\mathrm{i}\omega t + (\mathrm{e}^{\mathrm{i}\omega t} - 1)(n(\omega) + 1) + (\mathrm{e}^{-\mathrm{i}\omega t} - 1) n(\omega) \right] \mathrm{d}\omega \right\}. \tag{4}$$

In (4), $n(\omega)$ is the Bose–Einstein factor at temperature T, and $\beta(\omega)$ is a coupling strength function

$$g(\omega) = \sum \frac{|B_\nu|^2}{\hbar^2\omega_\nu^2}\delta(\omega - \omega_\nu).$$

The first few moments of $g(\omega)$ give the strength $\overline{n}$ of shake-up phonons, the lattice relaxation energy $\Delta\varepsilon$, and the RMS width Δ, $\overline{n} = \langle\omega^0(2n(\omega)+1)\rangle$, $\Delta\varepsilon = \hbar\langle\omega\rangle$, and $\Delta^2 = \hbar^2\langle\omega^2(2n(\omega)+1)\rangle$. When the temperature is high compared with the vibrational frequencies, the Bose factors are linear in T which leads to a RMS broadening $\propto\sqrt{T}$.

In the simplest case of one mode (e.g. a diatomic molecule), we have

$$D_{ph}(t) = \exp\{g(-\mathrm{i}\omega_0 + \mathrm{e}^{\mathrm{i}\omega_0 t} - 1)\} = \mathrm{e}^{-\overline{n}}\mathrm{e}^{-\mathrm{i}\Delta\varepsilon t/\hbar}\{1 + g\mathrm{e}^{\mathrm{i}\omega_0 t} + (g^2/2!)\mathrm{e}^{2\mathrm{i}\omega_0 t} + \ldots\}$$

and the broadening consists of discrete replicas at $-\varepsilon_0 - n\hbar\omega_0$ with a Poisson strength distribution, see e.g. [3, 20]. In the opposite limit of many modes appropriate for solids, the broadening tends to a Gaussian with increasing $\overline{n}$ [3]. The large $\overline{n}$ limit is also the classical limit where the core-hole broadening reflects the randomness of instantaneous ion positions when the core-level process occurs.

In higher order, the core hole will mix different modes, and the vibrational energies in the initial and final states will differ. Although the Franck–Condon overlaps for each mode can still be done exactly as long as we stay in the harmonic approximation, there is no simple representation like (4) for infinitely many modes. For solids, one would thus consider a finite but large number of modes, and then work out the required overlaps. A neat way of doing this has been introduced by Mäder and Baroni [19]. The low-order moments are readily found once the couplings are known. In particular, the RMS broadening is given by $\Delta^2 = \langle 0|\, V_{ph}^2\,|0\rangle - \langle 0|\, V_{ph}\,|0\rangle^2$. In the limit of high temperature, a quadratic coupling gives a contribution $\propto T$ to the RMS broadening.

Let us next turn to the electronic degrees of freedom and to shake-up of valence electrons. The basic expression (2) is of the form of a generic Franck–Condon problem with overlaps between no-hole initial states and final states perturbed by the core hole. Rather than attempting a direct perturbation expansion of the core-electron spectrum we following Langreth [15] expand in cumulants, i.e., make the *ansatz* $A_c(t) = \mathrm{e}^{C(t)}$, and expand $C(t)$ in powers of the core-hole perturbation V, $C = C_1 + C_2 \ldots$. The first-order term gives the 'initial state effects' and is given by

$$C_1(t) = i\,\langle 0|\, V\,|0\rangle\, t \approx -i\,\langle c|\, V_C\,|c\rangle\, t$$

(V_C is the total ground-state Coulomb potential from valence electrons and surrounding nuclei) and gives merely a shift but no broadening of the core line. The first moment thus gives a Koopmans value, a result known as the Manne–Åberg theorem [13] (see also Nozières [21]). The second-order term C_2 gives core-shifts and shake-up to linear-screening order and is formally identical to the phonon broadening function in (4). This similarity reflects the bosonic character of particle-conserving electronic excitations (particle-hole pairs, plasmons, etc). The coupling strength function g involves the dynamical structure factor S for the valence electrons and the bare core-hole potential,

$$g(\omega) \equiv \alpha(\omega)/\omega = \int \mathrm{d}^3r\mathrm{d}^3r' w(\boldsymbol{r})w(\boldsymbol{r}')S(\boldsymbol{r},\boldsymbol{r}'\omega)/(\hbar^2\omega^2)$$

where we following Minnhagen [22] have introduced an asymmetry function $\alpha(\omega)$. The first-order moment of g gives the core-hole relaxation energy to linear-screening order,

$$\Delta\varepsilon_c = \int \omega g(\omega)\mathrm{d}\omega = \int wS(\omega)w\mathrm{d}\omega/\omega = \tfrac{1}{2}v^{-1}(1 - \varepsilon^{-1}(\omega = 0))w. \qquad (5)$$

The moment of order zero gives the mean number of shake-up bosons $\overline{n}$. For insulators, the zeroth-order moment is well behaved, but for metals the Fermi surface makes $\alpha(\omega)$ tend to a constant for small ω and $\overline{n}$ diverges logarithmically owing to creation of low-lying particle-hole pairs. The fully relaxed hole state for metals is thus orthogonal to the ground state (the Anderson orthogonality catastrophe [23]). The no-boson line is then completely suppressed, the shake-up structure extends all the way to threshold, and the lineshape acquires a power-law form close to threshold,

$$A_c(\varepsilon) \sim \frac{\text{const}}{|\varepsilon - \varepsilon_c|^{1-\alpha(0)}}.$$

Further away from threshold, the intrinsic spectrum contains plasmon satellites carrying typically some 30% of the oscillator strength in simple metals. The plasmons contribute the major part of the core-hole relaxation energy in (5).

The higher-order terms in the cumulant expansion are not believed to give qualitative changes. Thus, to infinite order the relaxation energy will involve non-linear screening, and in metals the power-law behaviour near the edge remains, but with an asymmetry parameter α of all orders in the bare core-hole potential. In the case of simple metals the corrections beyond linear screening to the relaxation energy and asymmetry has been estimated to be 10% or less [24]. The smallness of the higher-order corrections is probably a consequence of that the core hole is fully screened already to linear order.

The formal similarity between the electron and phonon shake-up is valid also at finite temperatures. Thus (4) also yields the electronic part to order C_2 provided we choose $g(\omega) = \alpha(\omega)/\omega$. In metals, the Fermi singularity ($\alpha(0) \neq 0$) gives a thermal broadening with RMS width $\pi kT(\alpha(0)/3)^{1/2}$ [25].

So far we have neglected any internal structure of the core hole, which allowed us to treat it more or less as an external perturbation. In reality, the hole has $2j + 1$ magnetic sublevels which may be mixed with one another by interactions and split by a symmetry-breaking crystal field. Typically the energy scale is small, of the order 0.1 eV or less and visible only close to the edge. Thus, only states close to the relaxed hole state are of importance, and consequently, to a first approximation, the effects of core-hole degeneracy are to be evaluated with valence orbitals perturbed by the core hole. Owing to the greatly improved resolution available today, one can now begin to also see these finer details in the spectra.

Crystal field splitting is conceptually simplest to discuss. The non-spherical part of the crystal potential partially lifts the rotational degeneracy. These effects are usually very small in the bulk but may play a role at the surface. Consider for example a 2p core hole in the (100) surface layer of a cubic metal. The leading non-spherical components of the crystal potential at the core hole are $V_{10} \propto z$ and $V_{20} \propto z^2 - r^2/3$. V_{10} couples in second order and V_{20} in first order and split the sublevel with $j = 3/2$ in two components ($|m| = 1/2$ and $|m| = 3/2$). The effect is usually very small but has been observed recently in high-resolution spectra of Al [26].

A more interesting effect is the mixing of different magnetic sublevels by core-valence interactions. Going back to (1) we see that the direct term is independent of the core-hole spin whereas the second exchange term is not. Via core-valence exchange interactions, an up-spin valence electron may thus be scattered in such a way that both the electron and the hole reverse their spins. The dynamics of the core hole can no longer be trivially eliminated in this spin-dependent problem, and no exact results are known. The status of the problem has been reviewed by Almbladh and Hedin [3] and little theoretical development has occurred since then.

As discussed above, a core-level spectrum has a well defined threshold when the internal structure of the core hole and its finite lifetime is neglected. This is still the case also when

the exchange coupling between different magnetic core sublevels is taken into account. Let us first discuss core holes of s symmetry. The exchange coupling gives a positive contribution to the second moment of the core spectrum, $\Delta_x^2 = \langle H_x^2 \rangle - \langle H_x \rangle^2$. Because the sharp threshold remains and because primarily particle-hole pairs are involved, the exchange coupling must increase the asymmetry of the core line. A cumulant approximation would also give a power-law form of this exchange part, whereas an analysis to leading logarithmic order by Kato *et al* [27] gives a logarithmic behaviour. After applying an additional broadening from lifetime and phonons, the two results give similar resulting lineshapes. Turning to core holes of p symmetry, the core-valence exchange will mix the sublevels with $j = 1/2$ and $j = 3/2$ in such a way that the entire spectrum exhibits a sharp upper threshold. Consequently, the $j = 3/2$ remains sharp with some additional asymmetry, whereas the $j = 1/2$ sublevel acquires some extra broadening. Consider next the combined effects of crystal fields and core-valence exchange. The exchange will again mix the different crystal-field-split components of the spectrum. Thus, the uppermost component will acquire some extra asymmetry, and the lower ones some extra exchange broadening. The exchange coupling also has measurable consequences for the decay of the core hole. For example, in x-ray absorption, the exchange coupling leads to deviations from the statistical 2:1 ratio of the $j = 3/2$ and $= 1/2$ components [28]; the $j = 1/2$ component will be strongly suppressed when the core-hole lifetime is long compared to the exchange scattering time.

Summing up this brief survey we would state that the current theoretical understanding of core-level photoemission in the sudden limit is at a rather mature level. Combining this understanding and other theoretical tools like DFT and response theory allow us to perform simulations of fundamental importance for the interpretation of experimental data.

3. Surface core-level shifts

The atoms in the surface layer of a solid clearly experience surroundings which differ from those of the bulk atoms and thus a difference in core-level binding energy is expected between surface and bulk atoms. This core-level binding shift between surface and bulk atoms is commonly known as the surface core-level shift (SCLS). Some intuitive observations may be made regarding the SCLS. The difference between bulk and surface atoms is in some sense larger for more open surfaces simply because of the larger number of broken bonds for such surfaces. Thus the surface core-level shift is expected to be larger for more open surfaces. This is in general confirmed by experiment, see e.g. [11] for an experimental and theoretical study of a number of 4d elements. Also second (and deeper) layer atoms experience surroundings, which differ from that of bulk atoms even in the more close packed surfaces where the nearest-neighbour coordination shell of a second layer atom is equal to that of bulk atoms. Thus also second (and deeper) layer atoms are expected to differ in their core-level binding energy from bulk atoms. However, the resulting binding energy shifts are expected to be smaller than the first layer SCLS based on the simple fact that the difference in surroundings is smaller. Thus it is only recently that core-level binding energy shifts of deeper layers are commonly observed although some prominent examples of such shifts were found almost a decade ago, as described below.

Finally, non-spherical parts of the potential for atoms in the surface region may as mentioned in the preceding paragraph lead to a further splitting of the spin-orbit components. For a p level, the $j = 1/2$ component does not split but may shift whereas the $j = 3/2$ component can split into two components as well as shift. Including the leading terms allowed by symmetry we calculate for the surface atoms of Al(100) a shift of $\sim$1.5 meV for both the $2p_{1/2}$ and the $2p_{3/2}$ levels and a splitting of $\sim$16 meV for the $2p_{3/2}$ level. As mentioned

previously, the relevant potential for these calculation is the one with the core hole present. If we perform the same calculation for the initial state potential without the core hole we obtain a split of ∼40 meV, that is, the same result as Wimmer *et al* [29] who also neglected the core hole. These effects of the crystal field have been included in the analysis of the Al(100) spectra described below.

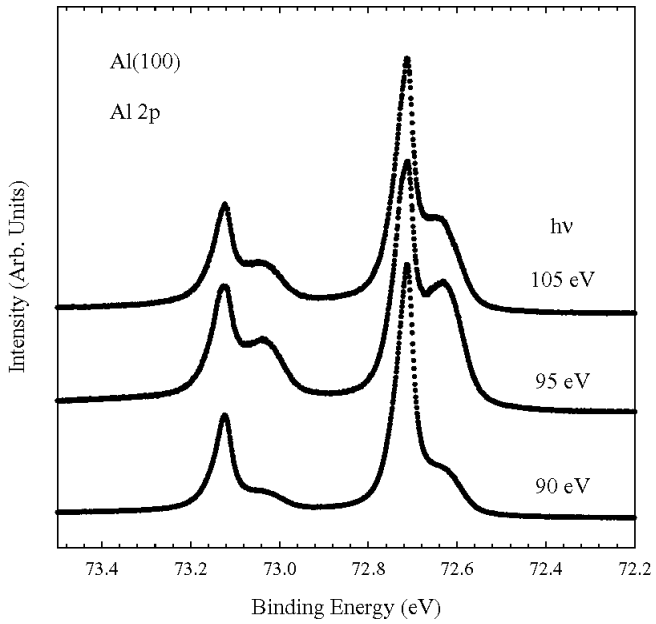

Figure 1. Normal emission Al 2p spectra at the indicated photon energies from an Al(100) surface. Measured at 100 K.

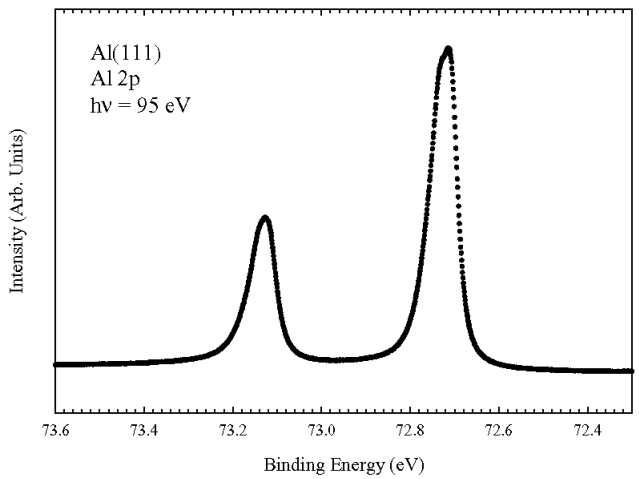

Figure 2. Normal emission Al 2p spectrum from an Al(111) surface. Measured at 100 K.

As an example of the SCLS of a metal and its variation with the crystallographic orientation of the surface we show in figure 1 and 2 Al 2p spectra for the Al(100) and Al(111) surfaces [26].

The surface and bulk components may be identified by varying the surface sensitivity of the measurements either by changing the mean free path of the photoelectrons via changing the photon energy (and thereby the kinetic energy of the electrons) as shown in figure 1 or by changing the polar angle of detection. The intensity variation with photon energy shown in figure 1 identifies the component at lower binding energy as the surface component of the Al(100) surface. A magnitude of ~ -95 meV (the $-$ sign indicates that the surface emission is at lower binding energy than the bulk) is derived for this SCLS. The Al(111) spectrum of figure 2 also depicts a double peak structure. This double structure is more pronounced for the $2p_{3/2}$ than for the $2p_{1/2}$ spin-orbit component due to the larger width of the $j = 1/2$ component caused by core-valence exchange. (We determine a width of the $j = 1/2$ component about 5 meV larger than for the $j = 3/2$ component.) The intensity ratio between the two components of the double structure shows a variation with photon energy which identifies the one at lower binding energy as surface related. Thus also the closepacked Al(111) surface shows a SCLS towards lower binding energy. However, the Al(111) surface core-level shift is, as expected, smaller than for the more open Al(100) surface and amounts to only ~ -28 meV. Close inspection of figure 1 shows that what we have so far termed the bulk peak for Al(100) actually also contains additional structure with a relative intensity that varies with photon energy. Figure 3 shows a comparison between the Al $2p_{3/2}$ spin-orbit components of the Al(111) and Al(100) surfaces. Clearly, the Al(100) spectrum contains in addition to the bulk and the aforementioned surface component a new component at slightly higher binding energy than the bulk component. From the intensity variation versus photon energy, this new component is identified as originating from the atoms of the second layer of the Al(100) surface and we thus measure a second layer core-level shift of $\sim +20$ meV for the Al(100) surface. These measured core-level shifts for the Al(111) and Al(100) surfaces compare favourably with calculated values. For Al(100) Feibelman [10] obtained a value of -97 meV for the SCLS using a Green function method in order to describe an isolated final state impurity. Using a slab and supercell based method we [26] obtain a value of -85 meV for the Al(100) SCLS, however, the magnitude of the calculated SCLS is found to depend almost linearly on the distance d_{12} between the first and second layers of the crystal. A decrease of d_{12}

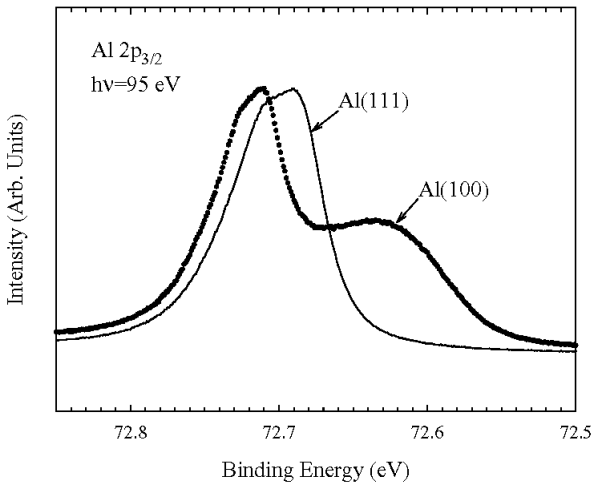

Figure 3. Comparison of the Al $2p_{3/2}$ region of Al 2p spectra from Al(111) (full line) and Al(100) dotted line). Measured at 100 K.

by 1% results in an increase of the calculated SCLS by about 10 meV and part of the difference between the present and the previous calculation by Feibelman actually derives from the fact that slightly different geometries are used in the two calculations. If we instead of the presently determined optimum d_{12} value use the value used in Feibelman's calculation we obtain a value of -105 meV. We would consider the level of agreement among the theoretical calculations as well as among theory and experiment to be quite remarkable. A similar level of agreement is also found for the SCLS of the Al(111) where we calculate a shift of -25 meV to be compared to an experimental value of ~ -28 meV. Finally for the second layer shift of the Al(100) we [26] obtain a theoretical value of +25 meV whereas for the Al(111) surface the calculations yield a very small second layer shift again in excellent agreement with experiment.

For most metallic surfaces the trends of the surface related core-level binding energy shifts are similar to those for the above aluminum surfaces. In particular, the second and deeper layers of close packed surfaces are normally found to exhibit only small binding energy shifts. This signifies that the core-level binding energy shifts are mainly sensitive to the nearest-neighbour surroundings of the ionized atoms and that the influence of the surface is screened out over a distance comparable to interatomic distances in most metals. However, a remarkable exception to this exists namely the close packed Be(0001) surface where not only the first but also the second and third atomic layers were experimentally shown to have 1s binding energies that differ significantly from the bulk value [30]. Later work [31] showed that even the fourth layer differed from the bulk value concerning the 1s binding energy. A Be 1s spectrum from the Be(0001) surface and its decomposition into such layer resolved components are shown in figure 4. The existence of such layer dependent core-level binding energy shifts of the Be(0001) surface was qualitatively confirmed by theoretical calculations at the time of their experimental discovery [32] and have since, although some temporary controversies existed [33], also been quantitatively confirmed [34] by *ab initio* calculations. Following the discovery for the Be(0001) surface, layer dependent core-level binding energy shifts were also experimentally found to exist on other low-index Be surfaces [35, 36]. Although some details of the assignment of the components for the Be($10\bar{1}0$) surface are still under discussion [37], there is general consensus that the surface related core-level binding energy shifts of Be extends far below the outermost layer and that the long range influence of the surface is caused by the unusually low density of states at the Fermi level of Be metal.

4. Adsorbate induced shifts

Clearly adsorption of foreign atoms or molecules on a surface will change the surroundings of the surface atoms and thereby cause the appearance of adsorbate induced binding energy shifts of the substrate core levels. The core-level binding energies of the adsorbate atoms are furthermore expected to depend on the adsorption site as different adsorption sites imply different local surroundings of the adsorbate. Measurements of core-level binding energy shifts of the adsorbate and the substrate atoms have proved to be very useful for obtaining information on the geometrical structure of many adsorbate systems. We will in this section give a few selected and hopefully instructive examples of this and refer the reader to e.g. [1, 7] for more examples.

The most obvious use of core-level photoemission in connection with molecular adsorption is to concentrate on the core levels of the adsorbate. As an example of this we show in figure 5 the development of the C 1s region as a Rh(111) surface is exposed to a background pressure of CO. At low CO exposures only a single C 1s component is seen indicating that only a single adsorption site is being taken by the CO molecules in the low coverage limit. At higher CO exposures, a second C 1s peak appears at lower binding energy indicating the onset of

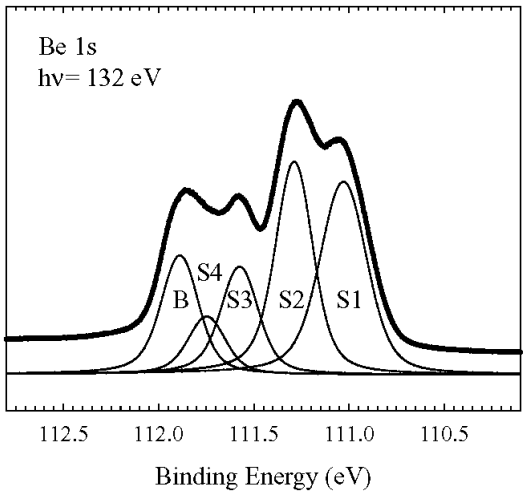

Figure 4. Normal emission Be 1s spectrum from a Be(0001) surface at an energy resolution of $\sim$ 70 meV. Measured at 100 K.

occupation of (at least) one new type of site at higher CO coverages. (This low binding energy peak actually turns out to contain two components at intermediate CO coverages. Very high-resolution measurements and a full analysis of the C 1s lineshapes [38] were needed in order to derive that the peak contained two components. This illustrates nicely that, strictly, core-level photoemission can only provide the lower limit for the number of inequivalent atoms as the shifts between some of the inequivalent atoms may be too small to detect.) The various C 1s components of figure 5 can be assigned to CO molecules in different adsorption sites on the Rh(111) surface. It turns out that the binding energies of these site specific components show no significant shifts with CO coverage indicating that the C1s binding energy of an adsorbed CO molecule is rather insensitive to the total CO coverage and thereby to the presence of CO neighbours on the surface. Thus the C1s binding energy seems to be a good fingerprint for the adsorption site of the CO molecules. This conclusion seems to be quite generally applicable for CO adsorption on metals; in the case of CO adsorption on Rh(111) it has been established not only for pure CO overlayers [39] but also for co-adsorption of CO with K [40] and O [41]. For these systems, large changes of the C 1s binding energies observed as a result of the co-adsorption were shown to result almost entirely from co-adsorbate induced changes of the CO adsorption sites. Clearly, such a fingerprinting property of core-level photoemission from the C 1s level of adsorbed CO is most valuable for studies of complicated co-adsorption systems as it allows for an easy determination of the CO adsorption sites. In this connection it is also important to notice that the core-level binding energy shifts of molecules in different adsorption sites can be calculated using the described *ab-initio* methods. For example, for the C 1s and O1s shifts between CO molecules in on-top and three-fold-hollow sites, respectively, on Rh(111) we [42] calculate values of 0.7 eV and 1.45eV in excellent agreement with the experimental values of 0.7 eV and 1.6 eV.

The relative intensities of the C 1s components carry information on the relative occupations of the possible adsorption sites. However, as the surroundings of the C atom in different sites differ, the diffraction of the outgoing relatively low-energetic photoelectrons is expected to be different thereby prohibiting a direct comparison of the intensities. That the effects of diffraction induced intensity changes may be significant is demonstrated in figure 6

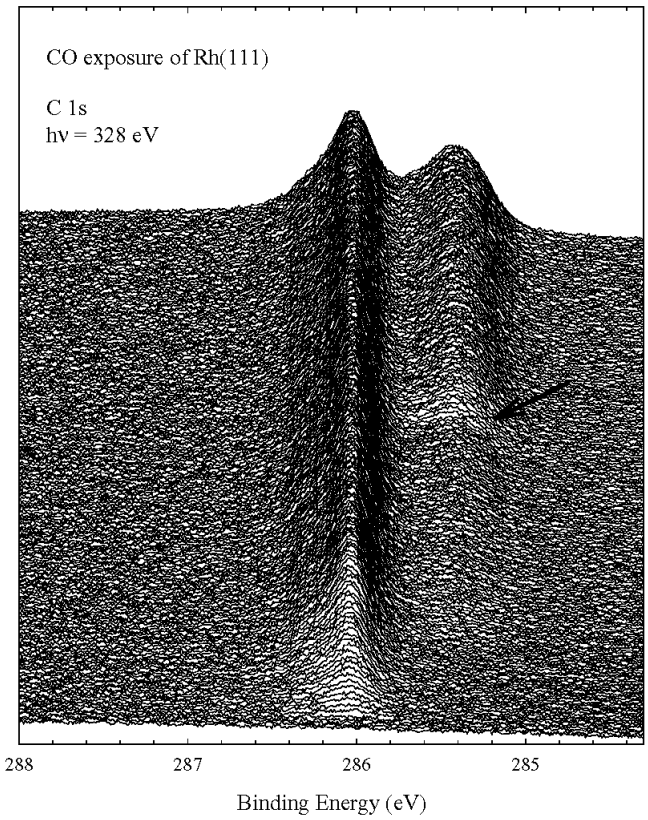

Figure 5. Normal emission C 1s spectra measured during exposure of a Rh(111) surface to CO at 220 K. Time per spectrum is 10 s. CO pressure is 4×10^{9} torr for the first ∼100 spectra after which it is increased to 4×10^{-8} torr at the point marked by the arrow.

which shows how the intensity ratio of the two components of normal emission C 1s spectra from a Rh(111)-(2 × 2)-3CO overlayer may be reversed simply by changing the photon energy from 350 eV to 380 eV. Thus it is necessary to calibrate the intensity-coverage relationship for the different adsorption sites (and photon energies) in order to make use of the relative intensities for deriving the relative site occupations. When such a calibration has been performed, the intensities of the different adsorbate components provide the relative occupation of the various adsorption sites. Combining this with the aforementioned fingerprinting character of the C1s binding energy for adsorbed CO allows for detailed quantitative studies [39–41] of site changes induced by e.g. changes of the total CO coverage and of the temperature and/or by co-adsorbates.

The core-level binding energy shifts of the substrate levels induced by the adsorbate often provide direct information on the molecular adsorption site. As an example of this we show in figure 7 Rh $3d_{5/2}$ spectra from a clean Rh(111) surface and a Rh(111)-($\sqrt{3} \times \sqrt{3}$)R30°-CO overlayer [39]. Comparing these two spectra, it is clear that about 1/3 of the surface Rh atoms change their core-level binding energy as a result of the adsorption of 1/3 monolayer of CO. This observation directly leads to the conclusion that the CO molecules adsorb in on-top sites as also found by more traditional structure determination techniques [43]. It may also be noticed that the core-level binding energy of the Rh surface atoms which do not bond to any

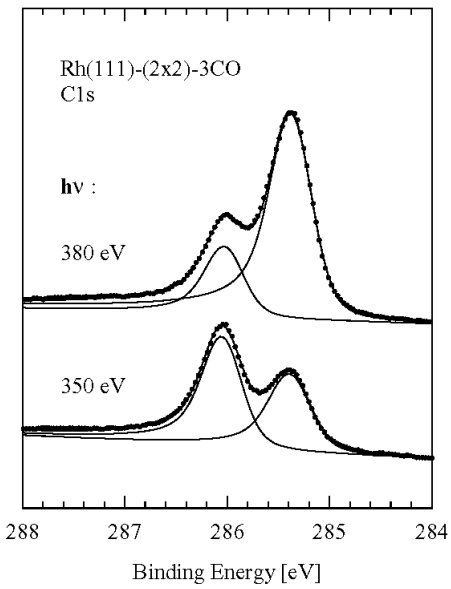

Figure 6. Normal emission C 1s spectra from a Rh(111)-(2 × 2)-3CO overlayer at two different photon energies. Measured at 100 K.

CO molecules remains very close to the value for the clean surface thereby demonstrating that in metallic systems core-levels shifts are normally dominated by nearest-neighbour effects. The CO induced shift of the Rh $3d_{5/2}$ level has been calculated by *ab initio* methods [42]. The use of the correct geometrical structure in such calculations turns out to be essential for this system in order to reproduce quantitatively the experimental results. For the Rh(111)-$(\sqrt{3}\times\sqrt{3})$R30°-CO structure, the on-top adsorbed CO molecules induce a significant buckling of the first Rh(111) plane where the Rh atoms underneath the CO molecules move outwards. A low energy electron diffraction study [43] yielded a value of 0.08 ± 0.06 Å whereas we [42] obtain a value of 0.19 Å from optimization of the total energy. If this buckling is *not* included in the core-level shift calculation we obtain a CO induced shift of about 0.5 eV (we give the shift relative to the bulk value) whereas if the buckling *is* included we calculate a shift of 0.24 eV in good agreement with the experimental value of 0.28 eV [42]. Thus the Rh $3d_{5/2}$ binding energy shift seems quite sensitive to the buckling of the outermost Rh layer and the experimental finding of CO induced shifts of similar magnitude for other overlayers with on-top CO molecules at low coverage indicates that a similar buckling occurs also for these overlayers.

The use of core-level photoemission sketched above for deriving adsorbate sites is also highly applicable to surfaces containing inhomogenieties either on an atomic or on a more mesoscopic length scale. For example, for adsorption on an alloy surface, only the alloy atoms which bond directly to the adsorbate are expected to experience a core-level binding energy shift whereby in the simplest case of on-top adsorption it is possible to determine directly if the adsorbate preferentially bonds to specific elements of the alloy. A similar simple reasoning also applies for adsorption on surfaces which are heterogeneous on a more mesoscopic length scale, e.g. islands of one material deposited on a surface of another material, as for instance reviewed in the article by Surnev *et al* [44] in this issue. Steps and other extended defects may also be regarded as inhomogenieties on a mesoscopic length scale and adsorption on these may be studied in a similar fashion provided of course that the step atoms have a sufficiently large binding energy shift that they can be resolved in the spectra.

High-resolution core-level photoemission has been used extensively for metal on metal

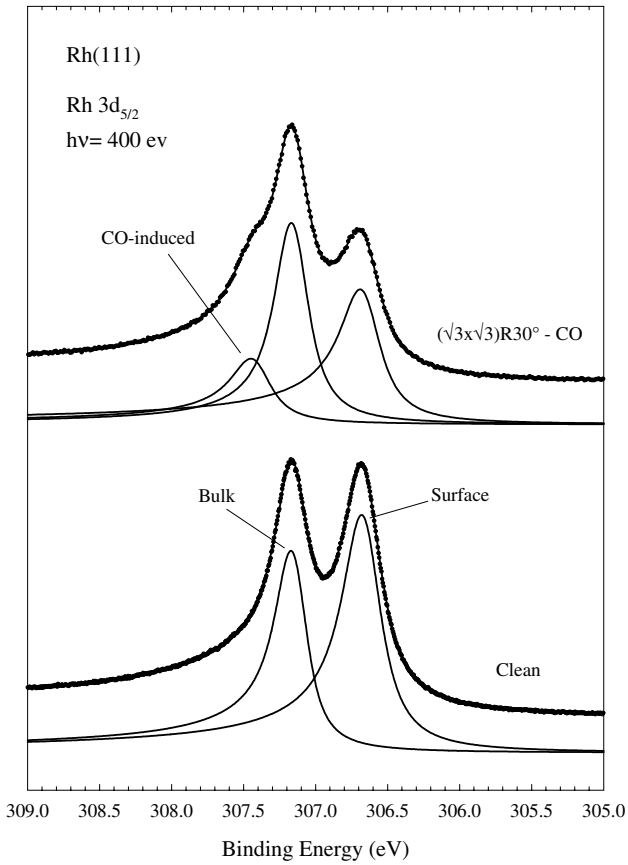

Figure 7. Normal emission Rh $3d_{5/2}$ spectra from clean Rh(111) and a Rh(111)-(3 × 3)R30°-CO overlayer. Experimental data are shown as dots. Decompositions into bulk and various surface related components and the resulting total line shapes are shown by full lines.

(and metal on semiconductor) systems where the technique facilitates studies of the growth during deposition of the metal film and of the possible alloy formation with the substrate. As an example of the use of high-resolution core-level photoemission for investigating the formation of (surface) alloys, we show in figure 8 Al 2p spectra for 0.5 ML of Na deposited on an Al(100) at 120 K. The lower spectrum is for the as-deposited overlayer whereas the upper one is measured after an anneal at 350 K. Both of these overlayers exhibit sharp $c(2 \times 2)$ LEED patterns, however, despite this similar long-range order the two Al 2p spectra immediately show that the detailed geometrical structure has changed as a result of the anneal [45]. In the as-deposited spectrum, Na adsorption is seen to mainly induce the appearance of a new Al 2p peak at about 150 meV lower binding energy than the bulk peak. The relative intensity of this peak is similar to that of the surface peak from the clean Al(100) surface. This spectrum is what would be expected for adsorption of the Na atoms in a fourfold hollow site on the Al(100) surface as such an adsorption geometry would make all Al surface atoms equivalent. The observation of two shifted components in the Al 2p spectrum measured after the anneal, however, shows that the annealed $c(2 \times 2)$ structure contains two inequivalent kinds of surface related Al atoms. This is what would be expected if the Na atoms substitute half of the Al atoms in the surface Al layer in a $c(2 \times 2)$ pattern. For such a structure, the Al atoms remaining

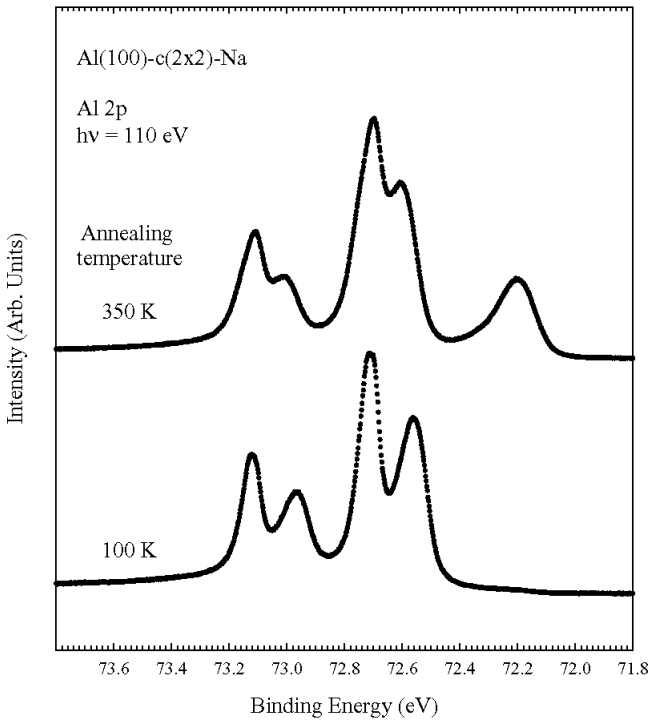

Figure 8. Normal emission Al 2p spectra from Al(100)-c(2 × 2)-Na overlayers. The lower spectrum is measured after deposition at 100 K without any further annealing whereas the upper spectrum is after an anneal at 350 K. Both spectra measured at 100 K.

in the first layer should show a large shift towards lower binding energy thus giving rise to the component at about −490 meV whereas the component shifted by about −100 meV can be attributed to Al atoms in the second layer [45]. *Ab-initio* calculations [46] of the Al 2p binding energy shifts confirm the above interpretations (which also agree with accepted structural models [47] of these overlayers). For the low temperature metastable structure with Na in a four-fold hollow site we calculate a binding energy shift of −170 meV for the first layer Al in good agreement with the experimental value of −150 meV. The experimental spectrum in figure 8 also shows a component at slightly higher binding energy (∼ +30 meV) than the bulk peak which is assigned to emission from the second Al layer. We calculate a shift of about +15 for both of the two kinds of second layer Al atoms in good agreement with the experimental value. Finally, it may be noticed that the weak component at large negative binding energy shift seen in the experimental spectrum can be ascribed to a small degree of intermixing even for this un-annealed surface. For the intermixed $c(2 \times 2)$ we [46] calculate Al 2p binding energy shifts of −450 meV and −90 meV for first and second layer Al atoms, respectively, again in excellent agreement with the experimental values of about −490 and −100 meV for these shifts. We believe that the level of agreement obtained for the present as well as for other systems is promising for a use of high-resolution core-level photoemission for not only monitoring the formation of alloys but also for deriving the detailed changes of the atomic geometry accompanying the alloy formation. Furthermore, such measurements may be performed in a time-resolved manner.

5. Vibrationally resolved core-level photoemission

The excitation of internal molecular vibration in the core-level photoemission process has for a long time been known to create finestructure in core-level photoemission spectra from molecules in gas phase [48]. The vertical nature of the core-level photoemission process results in a non-zero probability that the molecule is left in a vibrationally excited state after the photoemission event. The energy required for this excitation is taken from the kinetic energy of the outgoing photoelectron and the core-level photoemission spectrum will thus consist of several components each of which corresponds to a different number of vibrational quanta being excited in the final state molecule[3]. For molecules adsorbed on surfaces it is, however, only recently that such resolvable vibrationally induced finestructure has been observed experimentally [49] in core-level photoemission. With the improvements in the energy resolution obtainable at third generation synchrotron radiation facilities, however, observation of this finestructure is becoming more and more common [50]. Proper identification of the multiple components created by vibrational excitation is first of all important in order to avoid misinterpreting them as chemically shifted components. Secondly, their inclusion is also vital in any analysis of the core-level lineshape. Thirdly, the vibrational finestructure may in some cases provide important fingerprints of e.g. adsorption sites and hydrocarbon groups, see e.g. [49, 50].

The first observations [49] of excitation of internal molecular vibrations in core-level photoemission of adsorbed molecules were made for hydrocarbon overlayers on the Rh(111) surface. Figure 9 shows C 1s spectra from C_2H_3 and C_2D_3 molecules in a (2×2) overlayer on Rh(111). In these overlayers the ethylidyne molecules adsorb in a perpendicular geometry with one C atom bonding to the surface in a three-fold hollow site and the other being part of a methyl group [51]. The energy resolution of the spectra, which are from the original measurements [49], in figure 9 is only about 0.25 eV, however, even at this resolution both spectra clearly contain more than the two components expected solely from the presence of two inequivalent types of C atoms. Furthermore, the binding energies of some of the components at higher binding energy differ between the normal and the deuterated molecules. The interpretation of these spectra [49] is that the component at $\sim$283.4 eV is due to emission from the C atom bonding to the Rh surface atoms whereas all other components are due to emission from the C atom in the methyl group. The multiple components in the emission from the methyl group is caused by excitation of the C–H (or C–D) stretch vibration in the photoemission process. For the C_2H_3 overlayer, the component at 284.00 eV corresponds to the final state molecule being left in the vibrational ground state whereas the peaks at about 0.4 and 0.8 eV higher binding energy corresponds to excitation of one and two, respectively, quanta of the C–H stretch mode. For the deuterated case, the experimentally determined energy of this mode is lowered by a factor of close to $\sqrt{2}$ as expected for a harmonic oscillator potential and the effective mass increase of a factor of two caused by the deuteration of the molecule.

With the much better energy resolution achievable at third generation synchrotron light sources, similar finestructure caused by internal molecular vibrations are nowadays often [50] being found also for molecules with smaller vibrational energies like e.g. CO. Fine structure created by vibrational excitation may in many cases overlap with structure created by chemical shifts making it vital to correctly describe the vibrational lineshape when decomposing the spectra into chemically shifted components. In this connection it is important that the intensities of the vibrational progression for internal modes of chemisorbed

[3] Note that the relevant vibrational energy here is that of the final state core ionized molecule. Therefore the vibrational energies of core level photoemission are not equal to those found in traditional vibrational spectroscopies which measure the vibrations of the non-ionized ground state.

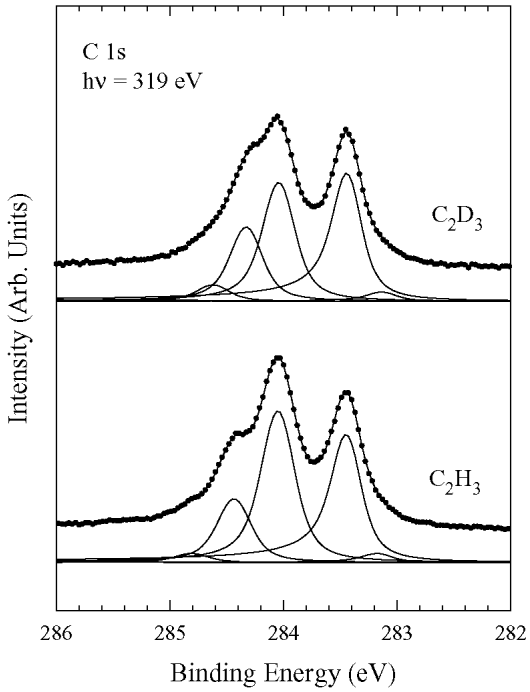

Figure 9. Normal emission C1 s spectra from Rh(111)-(2 × 2)-C2H3 and Rh(111)-(2 × 2)-C2D3 overlayers. Measured at 100 K.

(and free) molecules experimentally is found to be well described by a Poisson distribution as expected from a linear coupling model [3, 20] with the initial state molecules in the vibrational groundstate. The vibrational energies of the relevant modes are normally so large that excitations of them in the initial state may be neglected; i.e. the vibrational fine structure does not change with temperature. Furthermore, the vibrational replicas are normally equally spaced i.e. no significant anharmonicity of the final state potential is detected and all individual vibrational finestructure components have the same lineshape. These properties of the vibrational finestructure significantly reduce the number of free parameters and thereby increase the reliability of decompositions of complicated spectra.

Clearly a lineshape analysis which does not take into account the internal molecular vibrations will yield incorrect lineshape parameters. In many cases the vibrational finestructure creates additional emission on the high-energy side of a main peak which if not resolved and included in the analysis may be misinterpreted as a large asymmetry of electronic origin. As an example of this we return to the ethylidyne overlayers on Rh(111). In the original study [49] it was concluded that the inner C atom had a larger asymmetry index than the outer one which seemed intuitively reasonable as this atom is closer to the electron gas of the metallic substrate. Measurements [52] at higher energy resolution, however, show that the original finding of a large asymmetry index of the inner C atom was due to failure to include all internal vibrational modes. In figure 10 we show C 1s spectra of ethylidyne at an energy resolution of about 50 meV. At this resolution it is, in particular at a photon energy of 350 eV where diffraction effects suppress the intensity of the outer C atom emission, clear that the inner C atom peak contains an additional weak component shifted by about 140 meV towards higher binding energy. This component has been [52] tentatively assigned to excitation of the C–C stretch mode.

Irrespective of the detailed assignment of this vibrational finestructure, the failure to resolve and include it in the original analysis caused a too large value for the asymmetry index of the inner C atom. If included, the asymmetry index of the inner C atom is lowered considerably and no significant differences between the two C atoms can be determined regarding the asymmetry of the core-level lineshapes [52].

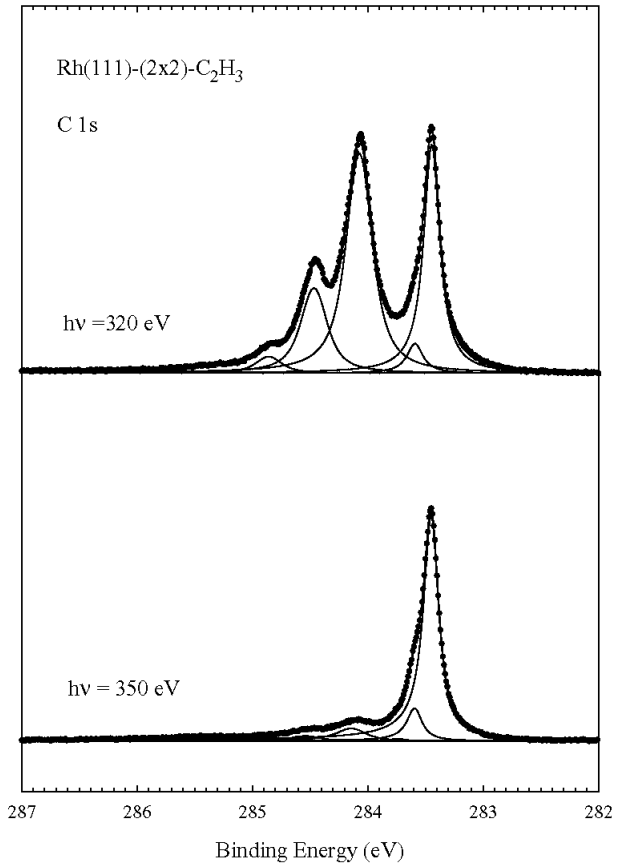

Figure 10. Normal emission C1 s spectra from a Rh(111)-(2 × 2)-C2H3 overlayer at the two indicated photon energies. Measured at 100 K.

Whereas it may not be too surprising that excitation of localized internal molecular vibrations creates finestructure in core-level photoemission spectra of adsorbed molecules, excitation of phonons is commonly [1,53] assumed to yield a structureless contribution to the broadening of the photoemission lineshape. In the limit of excitation of many phonons this broadening is well described by convolution with a Gaussian [1,3,53]. A recent experiment [54] has, however, demonstrated that for the case of Be metal the core hole couples to only a small part of the phonons which results in the formation of resolvable features in high-resolution Be 1s spectra. We show in figure 11, experimental Be 1s spectra measured at a resolution of about 20 meV from the Be(0001) surface. In addition to the aforementioned structure caused by the layer dependent Be 1s binding energies for the first few layers of this surface, the spectra also contain a strong finestructure when measured at this high resolution. Similar fine structure is also observed in Be 1s spectra from Be($10\bar{1}0$) and Be($11\bar{2}0$) surfaces [55]. The fine structure

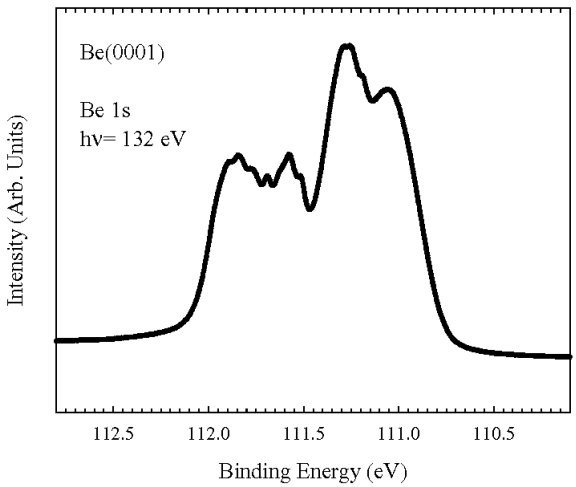

Figure 11. Normal emission Be 1s spectrum from a Be (0001) surface at an energy resolution of ∼20 meV. Measured at 100 K.

thus is a fundamental property of the 1s lineshape in photoemission from Be metal. The observed fine structure of the spectra can be reproduced if each of the layer components is taken to consist of a number of components having slightly different binding energies. For the surface layer no fine structure is visible and this layer is well described by a single broad component. The model functions used [54] for the emission from a single layer consist of a number of components positioned equidistant in binding energy $E_B(i) = E_B(1) + (i-1)\Delta E$, $i = 1$ to 7 where $\Delta E \sim 58$ meV corresponding to excitation of 0 to 6, respectively, phonons with an energy around 58 meV in the photoemission process. This line shape is shown in figure 12 for parameter values appropriate for the bulk emission of Be. Thus the coupling between the Be 1s core hole and the Be phonons is strongly peaked at phonon energies around 58 meV making the spectrum appear much like what would be expected for e.g. a molecule with an internal stretch vibration of around 58 meV. The coupling to the phonons gives a no-phonon line and a number of phonon replicas with intensities which follow a Poisson distribution rather closely. In contrast to the molecular case, however, the Be phonon replicas increase in width with increasing phonon replica number due to a finite width of the phonon band to which the core hole couples. The quite large intensities found even for highly vibrationally excited states are also understandable. The core-hole–lattice coupling reflects directly the core-hole induced forces on neighbouring sites, or, alternatively, the changes in equilibrium positions when a static core-hole impurity is introduced. In the case of 1s photoemission of metallic Be, Feibelman [33] has argued that the final state Be atom has a distance to its nearest-neighbour Be atoms which is ∼0.3 Bohr larger than the equilibrium distance. Such a large misfit corresponds to a quite strong coupling to the lattice. These qualitative arguments concerning the coupling strength are furthermore being supported by on-going [56] quantitative *ab initio* calculations.

Clearly, the vibrational fine structure must be included in a lineshape analysis of Be 1s in order to derive correct parameter values. For example, earlier studies used lifetime widths for the Be 1s core hole of ∼70 meV [30, 31] or ∼90 meV [30] whereas decompositions of the present spectra show this width to be around 50 meV in good agreement with a value of 40 meV obtained in a previous theoretical calculation by Almbladh *et al* [57]. In passing we note that the relevant charge density to use for the calculation of the decay is the one obtained in

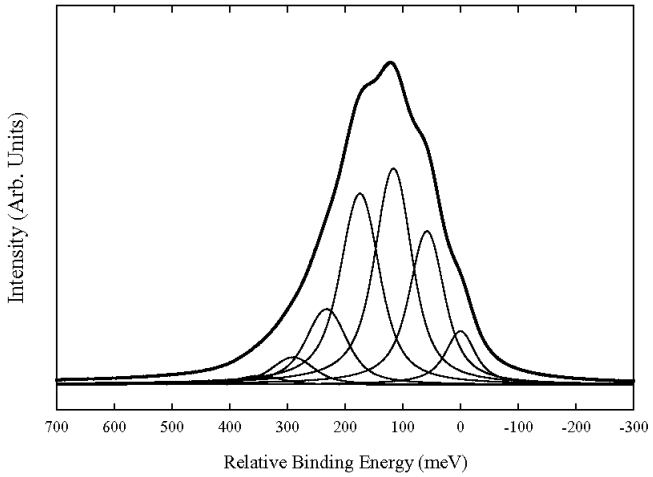

Figure 12. The model lineshape used for the decompositions of the vibrationally resolved Be 1s spectra. The lineshape is shown using parameters appropriate for the bulk emission.

the presence of the core hole, i.e. for the decay probability an initial state rule applies. For the case of Be, core-hole relaxation increases the lifetime width by a factor of three.

Whereas phonon induced replicas may be particularly prominent in Be metal because of the large phonon energies of Be [58], structures due to phonon excitation are nevertheless to be expected in other metals as well. As an example of this we show in figure 13 an Al $2p_{3/2}$ spectrum from Al(111) measured at a photon energy of 82 eV and a temperature of 100 K. Due

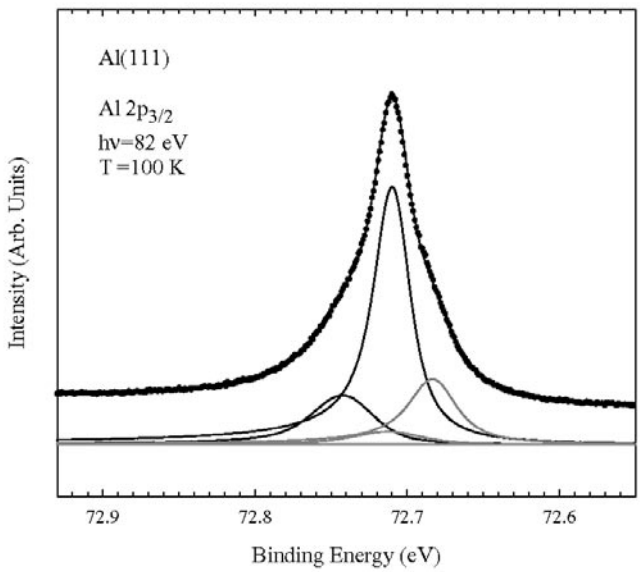

Figure 13. Normal emission Al $2p_{3/2}$ spectrum from an Al(111) surface measured at 100 K. Experimental data are shown as dots. Full lines shown decompositions into bulk (black) and surface (dark grey) components and the resulting total line shape.

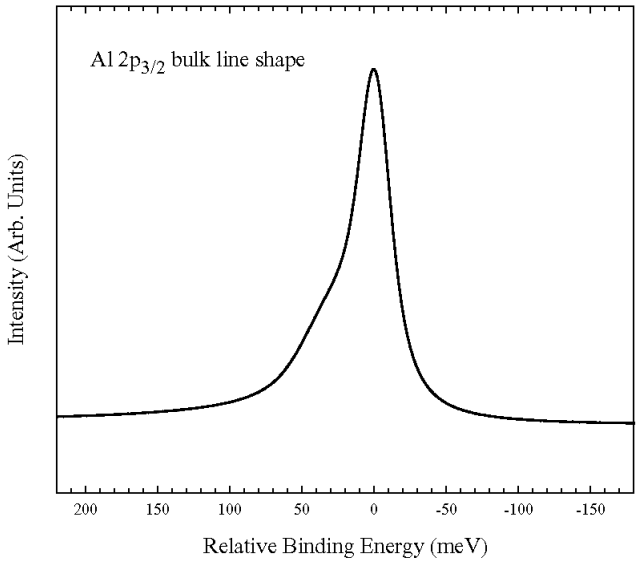

Figure 14. The Al $2p_{3/2}$ lineshape derived from the spectrum in figure 13.

to the bulk sensitivity at this photon energy, the surface peak is seen only as a weak shoulder on the low binding energy side of the bulk peak thereby minimizing the influence of any surface related features. As seen from figures 13 and 14, the bulk peak exhibits a double structure with one very sharp component and a broader emission feature at slightly higher binding energy. This is exactly theshape expected for a case with only weak coupling to the phonons [3]; a dominating no-phonon line and a weak structure at higher binding energy due to phonon losses (We neglect the phonon gain possibility at 100 K.) The Al case was actually calculated quite some time ago by Hedin and Rosengren [59] who found that on average about 0.6 phonons were excited per 2p photoemission event to be compared to an experimental value of about 0.3. Excellent agreement between theory and experiment can be obtained simply by rescaling these early results in order to take into account the slightly weaker coupling found in the experiment. These calculations based on linear coupling are, however, not able to reproduce the experimental spectra at higher temperatures where quadratic coupling is known [60] to be important for Al. Work aimed at going beyond linear coupling in calculations of the detailed lineshape for Al is in progress [61]. Finally we note that an excellent level of agreement between theory and experiment is also obtained for the lifetime width of the Al $2p_{3/2}$ level where a value of 22 meV has been calculated [57] whereas the decomposition included in figure 13 uses a lifetime width of 23 meV. (In addition to the lifetime width, the width of the no-phonon line only involves the experimental resolution and a contribution due to thermal excitation of electron hole pairs [25] which for Al at 100 K may be estimated to about 8 meV.)

We believe that any decompositions of high-resolution Al 2p core-level spectra, like e.g. those previously shown for clean and Na covered Al surfaces, must include this phonon induced structure. If this is not done, incorrect values for the asymmetry index and the lifetime broadening result. However, it should be noticed that the coupling to phonons is expected to change if the local geometrical surroundings change thereby adding some difficulty to such decompositions. In the general case, careful attention has to be paid to the phonon effects. In particular this is the case for systems with a weak core-hole–phonon coupling like Al as

structure in the core-level peaks may appear which, if not included, could result in erroneous conclusions concerning the basic lineshape.

6. Summary

We have given a number of examples demonstrating the usefulness of high-resolution core-level photoemission for investigating surface related systems. Hopefully these examples have demonstrated that by combining high-resolution measurements with accurate theoretical calculations it is possible to derive information that would have been difficult to obtain by either theory or experiment on its own. The combination of recent developments in *ab-initio* based electron structure theory with the basic understanding of core-level photoemission developed several decades ago, allows for rather accurate theoretical predictions.

Acknowledgments

The work described in this review has involved a large number of collaborators and it is not possible for us to mention and thank all of them explicitly. We would, however, like to acknowledge long standing collabourations and useful discussions with Ralf Nyholm, Edvin Lundgren, David L Adams, Lars Hedin and Ulf von Barth without which much of the presently described work would not have been completed. This work has been financially supported by the Swedish Natural Science Research Council.

References

[1] Egelhoff W F Jr 1986 *Surf. Sci. Rep.* **6** 253 and references therein
[2] Siegbahn K, Nordling C, Fahlman A, Nordberg R, Hamrin K, Hedman J, Johansson G, Bergmark T, Karlsson S-E, Lindgren I and Lindberg B 1967 *Atomic, Molecular and Solid State Structure Studied by Means of Electron Spectroscopy* (Uppsala: Almqvist and Wiksells)
[3] Almbladh C-O and Hedin L 1983 *Handbook on Synchrotron Radiation* vol 1B ed E-E Koch (Amsterdam: North Holland)
[4] Åberg T and Howat G 1992 *Handbuch der Physik* vol 31 ed W Mehlhorn (Berlin: Springer) p 496
[5] Johansson B and Mårtensson N 1980 *Phys. Rev.* B **21** 4427
[6] Nilsson A, Eriksson B, Mårtensson N, Andersen J N and Onsgaard J 1988 *Phys. Rev.* B **38** 10357–70
[7] Mårtensson N and Nilsson A 1994 *Application of Synchrotron Radiation* ed W Eberhardt (Berlin: Springer)
[8] See e.g.
Miedema A R, de Boer F R, and de Châtel P F 1973 *J. Phys. F: Met. Phys.* **3** 1558
Miedema A R 1973 *J. Less-Common Met.* **32** 117
Miedema A R, Boom R and de Boer F R 1975 *J. Less-Common Met.* **41** 283
Miedema A R 1976 *J. Less-Common Met.* **46** 67
[9] Hohenberg P and Kohn W 1964 *Phys. Rev.* **136** B864
Kohn W and Sham L J 1965 *Phys. Rev.* **140** A1133
[10] Feibelman P J 1989 *Phys. Rev.* **B39** 4866
[11] Andersen J N, Hennig D, Lundgren E, Methfessel M, Nyholm R and Scheffler M 1994 *Phys. Rev.* B **50** 17525
[12] Gunnarsson O and Jones R O 1989 *Rev. Mod. Phys.* **61** 689
Gunnarsson O and Jones R O 1995 *Density-functional Theory* ed Gross E K U and Dreizler J M NATO ASI series B **337** (New York: Plenum)
Gunnarsson O and Jones R O 1996 *Density-functional Theory I* Topics in current chemistry vol **180** (Berlin: Springer-Verlag)
Gunnarsson O and Jones R O 1996 *Recent Developments and Aapplications of Density-functional Theory,* ed J M Seminario (Amsterdam: Elsevier)
Gunnarsson O and Jones R O 1998 *Density-functional Theory: Theory and Applications* ed D P Joubert Lecture notes in Physics vol 500 (Berlin: Springer)
[13] Manne R and Åberg T 1970 *Chem. Phys. Lett.* **7** 282

[14] Lundqvist B I 1967 *Phys. Kond. Mater.* **6** 193
Hedin L and Lundqvist S 1969 *Solid State Physics* ed F Seitz, D Turnbull and H Ehrenreich (New York: Academic) vol 23 p 1
[15] Langreth D C 1970 *Phys. Rev.* B **1** 471
[16] Berglund C N and Spicer W E 1964 *Phys. Rev.* **136** A1030 Berglund C N and Spicer W E 1964 **136** A1044
[17] Mahan G D 1976 *Phys. Rev.* **163** 612
Nozières P and DeDominics C T 1969 *Phys. Rev.* **178** 1097
Doniach S and Šunjic M 1970 *J. Phys. C: Solid State Phys.* **3** 285
[18] Pryce M H L 1966 *Phonons in perfect lattices with point imperfections* ed R W H Stevenson (Edinburgh: Oliver and Boyd) p 403
[19] See e.g.
Mäder K A and Baroni S 1997 *Phys. Rev.* B **55** 9649
[20] Cederbaum L S and Domcke W 1976 *J. Phys. Chem.* **64** 603
[21] Nozières P 1964 *Interacting Fermi Systems* (New York: Benjamin)
[22] Minnhagen P 1976 *Phys. Lett.* **56A** 327
[23] Anderson P W 1967 *Phys. Rev. Lett.* **18** 1049
[24] Almbladh C O and von Barth U 1976 *Phys. Rev.* B **13** 3307 see also [3] p 668
[25] Ferrell R A 1969 *Phys. Rev.* **186** 399
Almbladh C-O and Minnhagen P 1978 *Phys. Status Solidi* **85** 135
[26] Borg M *et al* to be published
[27] Kato A, Okoji A and Osaka Y 1970 *Prog. Theor. Phys.* **30** 275
Kaga H 1977 *J. Phys. Soc. Japan* **43** 1144
[28] Onodera Y 1975 *J. Phys. Soc. Japan* **39** 1482
[29] Wimmer E, Weinert M, Freeman A J and Krakauer H 1981 *Phys. Rev.* B **24** 2292
[30] Johansson L I, Håkansson H I P, Andersen J N, Lundgren E and Nyholm R 1993 *Phys. Rev. Lett.* **71** 2453
[31] Johansson L I, Glans P-A and Balasubramanian T 1998 *Phys. Rev.* B **58** 3621
[32] Aldén M, Skriver H L and Johansson B 1993 *Phys. Rev. Lett.* **71** 2457
[33] Feibelman P J 1994 *Phys. Rev.* B **49** 13809
[34] Feibelman P J and Stumpf R 1994 *Phys. Rev.* B **50** 17480
[35] Johansson H I P, Johansson L I, Lundgren E, Andersen J N and Nyholm R 1994 *Phys. Rev.* B **49** 17460
[36] Johansson L I, Håkansson H I P, Lundgren E, Andersen J N and Nyholm R 1994 *Surf. Sci.* **231** L219
[37] Lizzit S, Pohl K, Baraldi A, Comelli G, Fritzche V, Plummer E W, Stumpf R and Hofmann Ph 1998 *Phys. Rev. Lett.* **81** 3271
[38] Smedh M, Beutler A, Ramsvik T, Nyholm R, Borg M, Andersen J N, Duschek R, Sock M, Netzer F P and Ramsey M G *Surf. Sci.* in press
[39] Beutler A, Lundgren E, Nyholm R and Andersen J N 1997 *Surf. Sci.* **371** 382
Beutler A, Lundgren E, Nyholm R, Andersen J N, Setlik B J and Heskett D 1998 *Surf. Sci.* **396** 117
[40] Strisland F, Beutler A, Jaworowski A J, Nyholm R, (1994). Setlik B, Heskett D and Andersen J N 1998 *Surf. Sci.* **410** 330
[41] Jaworowski A J, Beutler A, Strisland F, Nyholm R, Setlik B, Heskett D and Andersen J N 1999 *Surf. Sci.* **431** 33
[42] Birgersson M *et al* to be published
[43] Gierer M, Barbieri A, van Hove M A, Somorjai G A 1997 *Surf. Sci.* **391** 176
[44] Surnev S, Netzer F and Ramsey M 2001 *J. Phys.: Condens. Matter* **13**
[45] Andersen J N, Lundgren E, Nyholm R and Qvarford M 1992 *Phys. Rev.* B **46** 12784
[46] Borg M *et al* to be published
[47] Berndt W, Weick D, Stampfl C, Bradshaw A M and Scheffler M 1995 *Surf. Sci.* **330** 182
[48] Gelius U, Svensson S, Siegbahn H, Basilier E, Faxälv Å and Siegbahn K 1974 *Chem. Phys. Lett.* **28** 1
[49] Andersen J N, Beutler A, Sorensen S L, Nyholm R, Setlik B and Heskett D 1997 *Chem. Phys. Lett.* **269** 371
[50] See e.g. Wiklund M, Jaworowski A, Strisland F, Beutler A, Sandell A, Nyholm R, Sorensen S L and Andersen J N 1998 *Surf. Sci.* **418** 210
Föhlisch A, Wassdahl N, Hasselström, Karis O, Menzel D, Mårtensson N and Nilsson A 1998 *Phys. Rev. Lett.* **81** 1730
Föhlisch A, Hasselström, Karis O, Väterlein, Mårtensson N, Nilsson A, Heske C, Stichler M, Keller C, Wurth W and Menzel D 1999 *Chem. Phys. Lett.* **315** 194
[51] Koestner R J, Van Hove M A and Somorjai G A 1982 *Surf. Sci.* **121** 321
[52] Wiklund M, Beutler A, Nyholm R and Andersen J N 2000 *Surf. Sci.* **461** 107
[53] See e.g.
Wertheim G K and Citrin P H 1978 *Photoemission in Solids I* ed Cardona M and Ley L (Topics in Applied

Physics, Springer, Berlin)
[54] Andersen J N, Balasubramanian T, Almbladh C O, Johansson L I and Nyholm R 2001 *Phys. Rev. Lett.* **86** 4398
[55] Balasubramanian T *et al* unpublished results
[56] de Gironcoli S, Vast N, Birgersson M, Almbladh C-O *et al* unpublished
[57] Almbladh C-O, Morales A L and Grossman G 1989*Phys. Rev.* B **39** 3489
[58] Stedman R, Amilius Z, Pauli R and Sundin O 1976 *J. Phys. F: Met. Phys.* **6** 157
[59] Hedin L and Rosengren A 1977 *J. Phys. F: Met. Phys.* **7** 1339
[60] Theis W and Horn K 1995 *Phys. Rev.* B **51** 7157
[61] Birgersson M *et al* to be published